Path planning for agricultural robots in wild livestock farm environments

Haixia Qi[1,2*], Jinzhuo Jiang[1], Chaohai Wang[1]

(1. *College of Engineering, South China Agricultural University, Guangzhou 510642, China*;
2. *Guangdong Laboratory for Lingnan Modern Agriculture, Guangzhou, Guangdong 510642, China*)

Abstract: Path planning for field agricultural robots must satisfy several criteria: establishing feeding routes, maintaining gentle slopes, approaching multiple livestock observation points, ensuring timely environmental monitoring, and achieving high efficiency. The complex terrain of outdoor farming areas poses a challenge. Traditional A* algorithms, which generate only the shortest path, fail to meet these requirements and often produce paths that lack smoothness. Therefore, identifying the most suitable path, rather than merely the shortest one, is essential. This study introduced a path-planning algorithm tailored to field-based livestock farming environments, building upon the traditional A* algorithm. It constructed a digital elevation model, integrated an artificial potential field for evaluating multiple target points, calculated terrain slope, optimized the search neighborhood based on robot traversability, and employed Bézier curve segmentation for path optimization. This method segmented the path into multiple curves by evaluating the slopes of the lines connecting adjacent nodes, ensuring a smoother and more efficient route. The experimental results demonstrate its superiority to traditional A*, ensuring paths near multiple target points, significantly reducing the search space, and resulting in over 69.4% faster search speeds. Bézier curve segmentation delivers smoother paths conforming to robot trajectories.

Keywords: field-based livestock farming, agricultural robots, path planning, A* algorithm, artificial potential field, Bézier curve segmentation

DOI: 10.25165/j.ijabe.20241704.8632

Citation: Qi H X, Jiang J Z, Wang C H. Path planning for agricultural robots in wild livestock farm environments. Int J Agric & Biol Eng, 2024; 17(4): 207–216.

1 Introduction

Animal welfare farming is gradually emerging as the predominant livestock production model in the context of smart farming. The objective of welfare farming for farm animals is to address the conflict between animal welfare and high-efficiency farming, supporting a reduction in production intensity and the promotion of intensive farming practices while creating added value for both animals and consumers[1]. Intensive farming, a globally prevalent agricultural production method, effectively meets the increasing human demand for meat, eggs, and dairy products. However, the living conditions and health of farm animals under this farming model have been severely neglected, resulting in comparatively lower meat quality when contrasted with semi-intensive farming practices[2,3].

Semi-intensive farming, typically conducted in unstructured outdoor conditions, aims to provide animals with a free and comfortable growth environment. Nonetheless, large-scale unstructured farming places a significant labor demand. Data from 2017 shows that the proportion of agricultural labor participation in the United States, Japan, Germany, and Russia was 1.66%, 1.28%, 3.49%, and 6.70%, respectively[4]. This trend has been consistently decreasing year by year, indicating that agricultural labor is on a declining trajectory. The need for "automation" is steadily increasing. In recent years, with the rapid advancement of next-generation information technologies such as the Internet of Things[5,6], big data[7], artificial intelligence[8], and intelligent equipment manufacturing[9], these technologies have been widely applied across various aspects of agricultural production. Consequently, modern smart farms can achieve end-to-end information sensing, quantitative decision-making, intelligent control, precision inputs, and personalized services for agricultural production and management[10].

The development of mobile robots for field-based livestock farming can fundamentally address issues such as labor shortages, high labor intensity, low efficiency, and the need to monitor multiple target points. Currently, there is considerable research focused on mobile robots for intensive livestock housing, including facilities such as cattle barns, sheep pens, and poultry houses. Notable examples include the "Poultry Patrol" developed in 2019, which is an autonomous robot that uses thermal infrared cameras to detect diseased or dead birds. It is equipped with visible light cameras and a rotary cultivator, providing features like remote monitoring, video recording, and litter management. By automating the detection and handling of dead poultry, the Poultry Patrol enhances detection efficiency and reduces human contact with deceased birds, thereby lowering the risk of disease transmission, improving animal welfare, and enhancing farm management safety. Additionally, these robots provide continuous monitoring, significantly reducing the frequency of manual inspections and labor costs[11]. Another remarkable development is "ChickenBoy" (2021), which is the world's first autonomous monitoring robot suspended from the ceiling, developed by the Spanish company FAROMATICS. It is equipped with temperature, humidity, carbon dioxide, and wind speed sensors, enabling extensive monitoring of the poultry house environment. Additionally, it employs a set of cameras (infrared and visible light cameras) to monitor dead birds and water dispensers and notifies the caretakers through mobile

Received date: 2023-11-08 **Accepted date:** 2024-06-23

Biographies: Jinzhuo Jiang, MS candidate, research interest: agriculture robot, Email: jjinzhuo@163.com; **Chaohai Wang**, MS candidate, research interest: agriculture robot, Email: charwang@stu.scau.edu.cn.

***Corresponding author: Haixia Qi**, PhD, Associate Professor, research interest: agriculture robot. College of Engineering, South China Agricultural University, Guangzhou 510642, China. Email: qihaixia_scau@126.com.

alerts. This round-the-clock automated monitoring significantly lowers labor costs and enhances the precision of coop management, thereby boosting production efficiency and animal welfare. Farmers have reported notable improvements in coop environments, more stable poultry health, and a roughly 15% increase in production efficiency following the deployment of "ChickenBoy"[12]. Furthermore, Feng and Wang have developed a robot composed of an autonomous navigation vehicle, a spraying unit, an information monitoring unit, and a control unit When operating autonomously, this robot is capable of inspecting and disinfecting the environment. The precise disinfection capability of this robot helps prevent disease spread, thereby improving animal health. In practical applications, this robot has increased disinfection efficiency by 50% and significantly reduced the incidence of disease outbreaks[13].

These advancements in mobile robot technology for livestock farming are significant steps toward addressing labor-related challenges and improving efficiency while enhancing animal welfare and farm management.

The research on the mentioned robots primarily focuses on intensive farming conditions. Semi-intensive farming, on the other hand, typically encompasses free-range farms with undulating terrain. These farms have a larger livestock area, necessitating the monitoring of both animals and the environment, as well as the provision of supplemental feeding, all of which demand significant labor input. The importance of path planning lies in its ability to assist robots in effectively navigating terrain obstacles and farm facilities. This enhances the efficiency of monitoring and feeding operations, reduces human labor requirements, and ensures optimal health and growth environments for livestock. Therefore, path planning algorithms tailored for semi-intensive farming are crucial for addressing labor shortages and improving farm efficiency.

In semi-intensive farming environments, there is currently a lack of path-planning solutions specifically designed for robots. This remains a challenging area due to the expansive terrain and variable topography typical of these farms, whereas existing path planning technologies are predominantly tailored for the structured environments of intensive farming operations. Mobile robots designed for use in intensive conditions typically rely on magnetic strips or guided tracks for path planning and are ill-suited for unstructured field-based livestock farming environments. In traditional vertex inspection processes, the shortest path between two points is typically used for path planning. However, in the free-range activity areas of livestock, animal behavior patterns often lack clear regularity. Therefore, path planning should prioritize proximity to the animals' activity areas to effectively monitor their growth environment and health status. Additionally, to improve the efficiency of feed supplementation, the feeding path should also closely follow the livestock activity areas. At the same time, to avoid causing unnecessary disturbance to the animals, mobile robots should maintain a certain distance while performing tasks, ensuring normal animal activities.

The current challenges of labor shortages and efficiency demands in agriculture have placed enormous pressure on semi-intensive farms, necessitating the development of more intelligent path-planning algorithms. The key challenge in path planning for field-based livestock farming robots lies in dealing with unstructured environments and the multi-target planning problem involving both environmental and livestock observation. Research in this area predominantly focuses on algorithm development. Wu et al.[14] improved the evaluation function and designed a path optimization algorithm that considers slope and roughness constraints by studying the comprehensive impact of terrain slope and surface properties on vehicle path planning. Ji et al.[15] employed a method for random sampling path planning based on off-road terrain information and constructed an evaluation function for off-road path planning in an autonomous vehicle context. Tian et al.[16] employed the artificial potential field algorithm to model off-road environments, assess vehicle traversal risks, and propose a probabilistic graph algorithm based on the potential field model. Zhao[17] combined passability grading and recommended vehicle speed to design an improved ant colony algorithm to achieve the shortest travel time. The algorithm optimized paths to simultaneously consider efficiency, passability, and safety. Wang et al.[18] established taboo lists for traversal and slope weight tables to narrow the search range, allowing for three-dimensional space path planning.

In the aforementioned research, this study introduced a path-planning algorithm tailored to field-based livestock farming environments, building upon the foundation of the traditional A-star (A*) path-planning algorithm. The key steps of this algorithm are as follows:

1) Digital Elevation Model (DEM) Construction: The algorithm commences by creating a Digital Elevation Model (DEM) based on the environmental characteristics of the livestock farming site. This DEM serves as a critical input for path planning, offering insights into the topography of the area.

2) Artificial Potential Field Evaluation: To navigate in the unstructured field environment and address the multi-target planning problem, the algorithm incorporates an artificial potential field as the evaluation function. This field takes into account the positions of multiple target points and guides the robot by exerting forces on it to move in the desired direction.

3) Optimization of Search Neighborhood: To ensure efficient and obstacle-free navigation, the algorithm calculates terrain slopes and evaluates the direction of the target points, thereby optimizing the search neighborhood. This step helps the robot select the most favorable path segments.

4) Bézier Curve Segmentation: Finally, the algorithm employs Bézier curve segmentation to further enhance the quality of the generated path. The Bézier curves create smooth and continuous paths, which are suitable for the movement of mobile robots, avoiding abrupt turns or rough trajectories.

This path-planning approach addresses the unique challenges of field-based livestock farming environments, ensuring that the robot can navigate complex and unstructured terrain while closely approaching multiple target points, and optimizing the path for efficient and smooth movement.

2 Materials and methods

2.1 Environmental modeling for field-based livestock farming

Before delving into path planning in field-based livestock environments, the establishment of a three-dimensional map is a crucial prerequisite. This map serves as the foundation for planning and provides a transformed, abstract representation of the real environmental scene that is manageable for the robot. Common methods for representing such maps include topological modeling, contour maps, and grid-based mapping. In conventional grid-based mapping, individual grid cells are assigned binary values of 0 and 1 to respectively denote the presence or absence of obstacles within a specific grid. Figure 1 shows an example of grid mapping, where black grid cells represent obstacles and white grid cells signify passable areas. This method is straightforward and easily extensible

to three-dimensional environments by employing grid cell data to represent spatial structures. When grid cells store height information, the resulting environment model is referred to as a Digital Elevation Model (DEM).

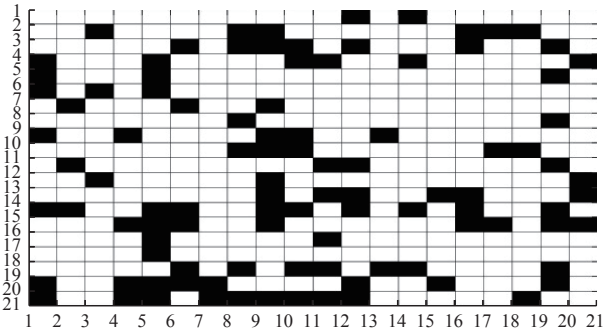

Note: Black grid cells represent obstacles and white grid cells signify passable areas.

Figure 1 Standard grid map used by the robot

Grid-based mapping offers a simple structure, facilitating the creation and maintenance of three-dimensional environmental spaces. It is especially capable of representing irregular obstacles, making it suitable for complex and ever-changing terrain in outdoor environments. In outdoor livestock farming scenarios, the importance of constructing a three-dimensional grid map cannot be overstated. By mapping the real environment into a detailed 3D grid map, path planning algorithms can obtain precise terrain data. This grid-based 3D modeling approach enhances the accuracy and efficiency of path planning, ensuring effective robot operation in complex terrains. Furthermore, 3D grid maps accurately reflect terrain undulations and obstacle distributions, providing essential topographical information for path planning. This results in paths that are more aligned with actual environmental needs, thereby improving the stability and reliability of robotic operations. Thus, exploring and utilizing the grid method for 3D modeling is crucial for path planning in outdoor livestock environments.

Given that this research focuses on unstructured, roadless field conditions with varied topography, grid-based mapping stands out as a preferred choice for creating a three-dimensional environment model. In this approach, elevation information is incorporated into the grid cells, culminating in the establishment of a three-dimensional elevation model that effectively simulates the field-based environment, as shown in Figure 2. This selection aligns with the complex and dynamic nature of field environments, allowing for accurate representation and navigation in such terrains.

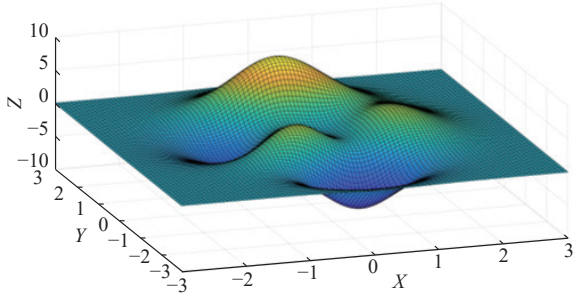

Figure 2 A detailed three-dimensional elevation model mapped from the field environment

2.2 Traditional A* algorithm

The A* algorithm, introduced by Hart and his colleagues[19], has found widespread application in the field of shortest-path problems. As a typical heuristic search algorithm, A* evaluates nodes using heuristic search, thereby improving the efficiency of node exploration. It is known for its strong performance and accuracy. A* utilizes a heuristic evaluation function for the heuristic search, which is represented as follows:

$$F(n) = G(n) + H(n) \tag{1}$$

where, $F(n)$ represents the total estimated cost from the starting position to the current position n to the target position, $G(n)$ represents the actual cost of the path from the starting position to the current position, and $H(n)$ represents the estimated cost from position n to the target position. The pathfinding process of the A* algorithm is shown in Figure 3. The dark green grid represents the starting point, the red grid indicates the endpoint, the gray grid represents obstacles, the white grid signifies traversable areas, the light green grid indicates the area to be searched, the blue grid shows the areas already searched, and the yellow line represents the currently discovered path.

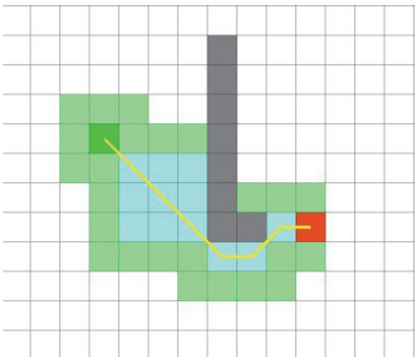

Note: The dark green grid represents the starting point, the red grid indicates the endpoint, the gray grid represents obstacles, the white grid signifies traversable areas, the light green grid indicates the area to be searched, the blue grid shows the areas already searched, and the yellow line represents the currently discovered path.

Figure 3 The pathfinding process of the A-Star algorithm on a conventional grid map

2.3 Improved A* algorithm

In practical applications, robots first plan their paths within the environmental mapping and then follow these paths. However, when using the traditional A* algorithm for path planning, the generated paths are typically the shortest ones, which do not conform to the requirements of closely approaching multiple points of livestock observation, maintaining gentle slope, aligning with supplemental feeding routes, and may result in excessive computation time. To address these issues, this paper combines the principles of artificial potential fields with the A* algorithm and introduces a new method for constructing a heuristic function. In the approach proposed in this study, the impacts of algorithm execution time and terrain slope on the robot were also considered, optimizing the search neighborhood. The new evaluation function is expressed as follows:

$$f(n) = g(n) + h'(n) \tag{2}$$

$$h'(n) = \alpha h(n) + \beta a(n) \tag{3}$$

where, $f(n)$ represents the total estimated cost from the starting position to the current position to the destination, $g(n)$ represents the path movement cost from the starting position to the current position[20]. Equation (3) was used as an improved heuristic function.

$h(n)$ represents the distance cost in traditional A*, and $a(n)$ represents the cost associated with the potential field of the livestock, which includes information about the surrounding livestock. α and β are the proportionality factors between $h(n)$ and $a(n)$.

$h(n)$ represents the distance cost d in traditional A*, and this calculation typically utilizes Manhattan distance, Euclidean distance, and diagonal distance. In this study, the Euclidean distance was used to calculate the cost of movement. For the three-dimensional space represented using grid-based mapping, the cost d is expressed as follows in Equation (4):

$$d = \sqrt{(x_g - x_i)^2 + (y_g - y_i)^2 + (z_g - z_i)^2} \quad (4)$$

where, g represents the position of the target point with coordinates (x_g, y_g, z_g), and i represents the current position with coordinates (x_i, y_i, z_i).

2.3.1 Multi-objective heuristic $a(n)$

Based on the principles of artificial potential fields, obstacles generate repulsive forces that decrease with increasing distance from the obstacle to the node. Conversely, target locations create attractive forces that are directly proportional to the distance from the node to the target. In this study, the environmental map was constructed as a grid-based map, with each grid location represented by coordinates. The potential field force is one of the evaluation functions in A*. In the grid-based map environment, the formula for calculating the repulsive force is as follows, with the direction being from livestock i to node k.

$$F_r = (k,i) = \begin{cases} \eta\left(\dfrac{1}{\rho(x_i,y_i)} - \dfrac{1}{d_0}\right)^2, & if\ \rho(x_i,y_i) \le d_0 \\ 0, & if\ \rho(x_i,y_i) > d_0 \end{cases} \quad (5)$$

$$\rho(x_i,y_i) = \sqrt{(x_k - x_i)^2 + (y_k - y_i)^2} \quad (6)$$

where, k represents the current position with coordinates (x_k, y_k), and i represents the ith grid containing livestock with coordinates (x_i, y_i). Considering that only robots near the livestock would disturb them, and in order to reduce computational load, this study restricted the range of livestock. $\rho(x_i, y_i)$ represents the distance from the current node k to the ith obstacle, and d_0 is the distance threshold. When the distance from the current point to the nearest livestock is greater than d_0, no repulsive force is generated. η is also a simple proportionality factor. In this study, the calculation of the magnitude of the attractive force is as Equation (7), with the direction from node k to the target point d.

$$F_a(k) = [(x_g - x_k)^2 + (y_g - y_k)^2] \quad (7)$$

where, k represents the current position with coordinates (x_k, y_k), and g represents the target point with coordinates (x_g, y_g). After obtaining the attractive and repulsive forces, the total force is calculated to determine the potential field experienced by the current grid node k. The calculation equation is as follows:

$$F(k) = \gamma F_a(k) + \mu \sum_i F_r(k,i) \quad (8)$$

In this context, γ and μ represent the weights of the attractive and repulsive forces, respectively. In this study, γ=1 and μ=3. Artificial potential field methods inevitably encounter the problem of local minima. When the calculated $F(k)$ is equal to 0, to avoid the algorithm reverting to the traditional A* algorithm, the repulsive force at that point was abandoned. At this point, the calculation equation for $F(k)$ is as follows:

$$F(k) = \gamma F(k) \quad (9)$$

As livestock served as multiple target points, the path needed to be close to the livestock but not excessively close. Therefore, the livestock coordinates were designated as both obstacle points and attraction points. When the distance to the livestock is beyond d_0=5 m, the attractive force increases, while within a range of d_0=5 m from the livestock, the repulsive force intensifies. The potential field for multiple target points is shown in Figure 4.

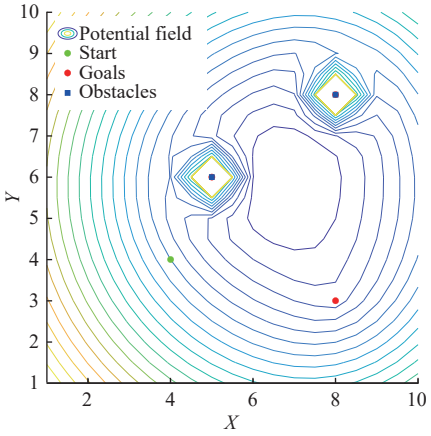

Figure 4 Potential field of multiple target points when obstacle points and target points coincide

2.3.2 Optimizing the search neighborhood

Traditional A* algorithm in a two-dimensional grid map checks whether the neighborhood is passable by examining whether there are obstacles within a grid. When the grid contains a value of 1, it indicates the presence of an obstacle, making the neighborhood impassable and excluded from the A* search list. Conversely, a value of 0 means the neighborhood is obstacle-free, allowing it to be added to the A* search list. In this study, a digital elevation model is used where the grid stores height information. As shown in Figure 5, the height of adjacent nodes may vary, and when the height difference is too large, the robot cannot pass through. Therefore, this study assessed neighborhood feasibility based on the maximum slope S that the robot can traverse, calculated as follows:

$$S = \arctan\left(\frac{z_d}{d_k}\right) \quad (10)$$

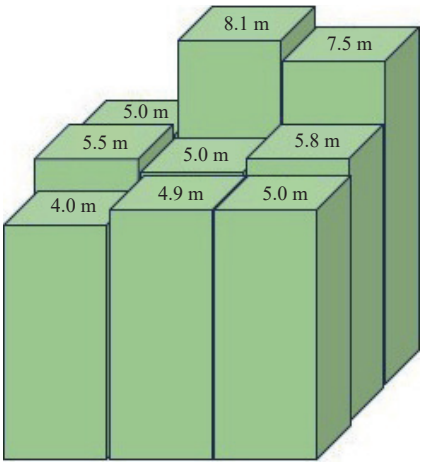

Note: Black The central square represents the current node, with the eight surrounding squares indicating neighboring nodes being evaluated. The numbers above the squares represent the height information of the current node.

Figure 5 Elevation grid schematic of adjacent nodes in the search neighborhood

$$z_d = |z_{k+1} - z_k| \tag{11}$$

$$d_k = \sqrt{(x_{k+1} - x_k)^2 + (y_{k+1} - y_k)^2 + (z_{k+1} - z_k)^2} \tag{12}$$

where, k represents the current position with coordinates (x_k, y_k, z_k), and k+1 represents an adjacent node in the search neighborhood with coordinates (x_{k+1}, y_{k+1}, z_{k+1}).

The traditional A* algorithm follows a search strategy that begins from the central node and expands into the eight surrounding neighborhoods to find the next node to expand, based on the evaluation function, as shown in Figure 6a. In this study, the search strategy has been adjusted to three neighborhoods based on the direction of the target node relative to the current node, as illustrated in Figure 6b. In this figure, node ⑤ serves as the central node, and based on the direction of the target node, 5 nodes are discarded while 3 nodes are added for expansion. For example, if the target node is located in the 0° to 90° direction from the central node, nodes ①, ④, ⑦, ⑧, and ⑨ are discarded, and only nodes in the 0° to 90° direction, such as nodes ②, ③, and ⑥, are included in the set of nodes to be expanded. This process continues for other angles in the same way. The expansion node is selected based on the comparison of the evaluation function values to find a more efficient path to the target point. However, the 3-neighborhood search strategy still has limitations. For instance, when the A* algorithm changes the search neighborhood from the traditional 8-neighborhood to a 3-neighborhood, it might encounter corner cases like the one shown in Figure 6c. In such situations, the algorithm might get stuck in a "trap". To address this, if obstacles appear in the set of nodes to be expanded corresponding to the target node, the 8-neighborhood search strategy is used as an alternative option, discarding the initial 3-neighborhood search strategy to enable the alternative 8-neighborhood search.

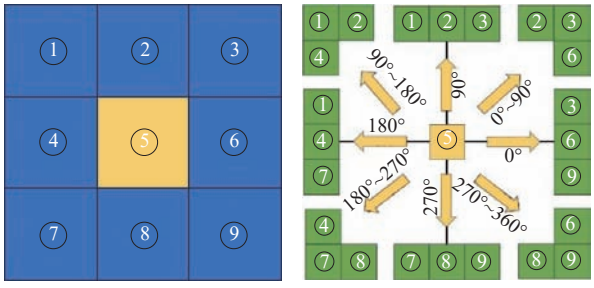

a. The nodes to be expanded are selected basedon the evaluation function

b. Adjusted to a three-neighborhood search based on the direction of the target node

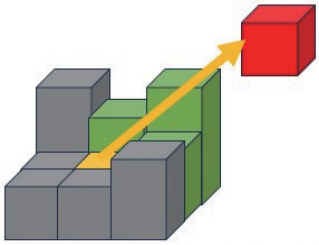

c. Deadlock situation when an obstacle coincides with the node to be expanded in the direction of the target node

Note: The yellow square represents the current node, the green squares indicate the nodes to be searched, the yellow arrow shows the direction of the target node, and the red square marks the target node.

Figure 6 Improvement of the traditional A* algorithm by replacing 8-neighborhood search with 3-neighborhood search oriented towards the target direction

2.4 Path Smoothing

In grid maps, the planned paths often contain numerous sharp turns and large corners, causing the mobile robot to make abrupt turns or even come to a complete stop during its motion. This unstable motion not only reduces the efficiency of the mobile robot's operation but also leads to increased power consumption and wear and tear. As a result, many researchers have started utilizing traditional Bézier curves to smooth the optimal paths generated during planning. Due to the poor numerical stability of high-order Bézier curves, this study employed piecewise third-order Bézier curves.

Bézier curves require just a few control points to generate more complex, smooth curves. This paper uses Bézier curves to achieve path smoothing on the optimal planned path. Typically, n+1 control points are defined to create an n-th order Bézier curve, as expressed in Equation (13).

$$P(t) = \sum_{i=0}^{n} P_i B_{i,n}(t), \ t \in [0,1] \tag{13}$$

In Equation (13), P_i and t represent the coordinate values of the control points and the parameter, respectively. $B_{i,n}(t)$ denotes the Bernstein polynomial, and its expression is defined in Equation (14).

$$P_i B_{i,n}(t) = C_n^i t^i (1-t)^{ni}, \ i = 0, 1, ..., n \tag{14}$$

In Equation (14), C_n^i represents the binomial coefficient, and n is the degree of the Bézier curve. The common parameter expressions for a third-order Bézier curve are as follows:

$$P(t) = P_0(1-t)^3 + 3P_1(1-t)^2 t + 3P_2(1-t)t^2 + P_3 t^3, \ t \in [0,1] \tag{15}$$

From Equation (15), it can be seen that a third-order Bézier curve passes through the first control point P_0 (t=0) and the fourth control point P_3(t+1).

When the complete path is obtained, the path is smoothed by checking the slope of the connecting lines between adjacent nodes. The specific process is as follows:

1) Connect adjacent nodes (m, m+1) and (m+1, m+2) in the path and check if the slope of the connecting line falls within the specified slope threshold range. If it does, add nodes (m, m+1, m+2) to the list of points to be smoothed and apply third-order Bézier curve smoothing. If the slope does not fall within the threshold range, set node m+1 as the new starting point.

2) Repeat Step 1 by iterating through all the path nodes until all nodes have been processed.

2.5 Fusion Algorithm

The algorithm fusion proposed in this study combines the improved A* algorithm with segmented third-order Bézier curves. It first utilizes the improved A* algorithm for path planning and then employs segmented Bézier curves to smooth the planned path, reducing redundant nodes and making the path smoother. The specific process of the fusion algorithm is shown in Figure 7.

3 Experiments

To validate the performance of the improved A* algorithm, this section conducted comparative simulation experiments on a Windows 11 operating system with an Intel i5-12400F processor and 16 GB RAM using Matlab R2020b.

The parameters required for the improved A* algorithm include the distance cost ratio factor α, the livestock potential field cost ratio factor β, the potential field repulsion coefficient η, the attraction weight γ, the repulsion weight μ, and the maximum slope S. The maximum slope S is determined based on the robot's

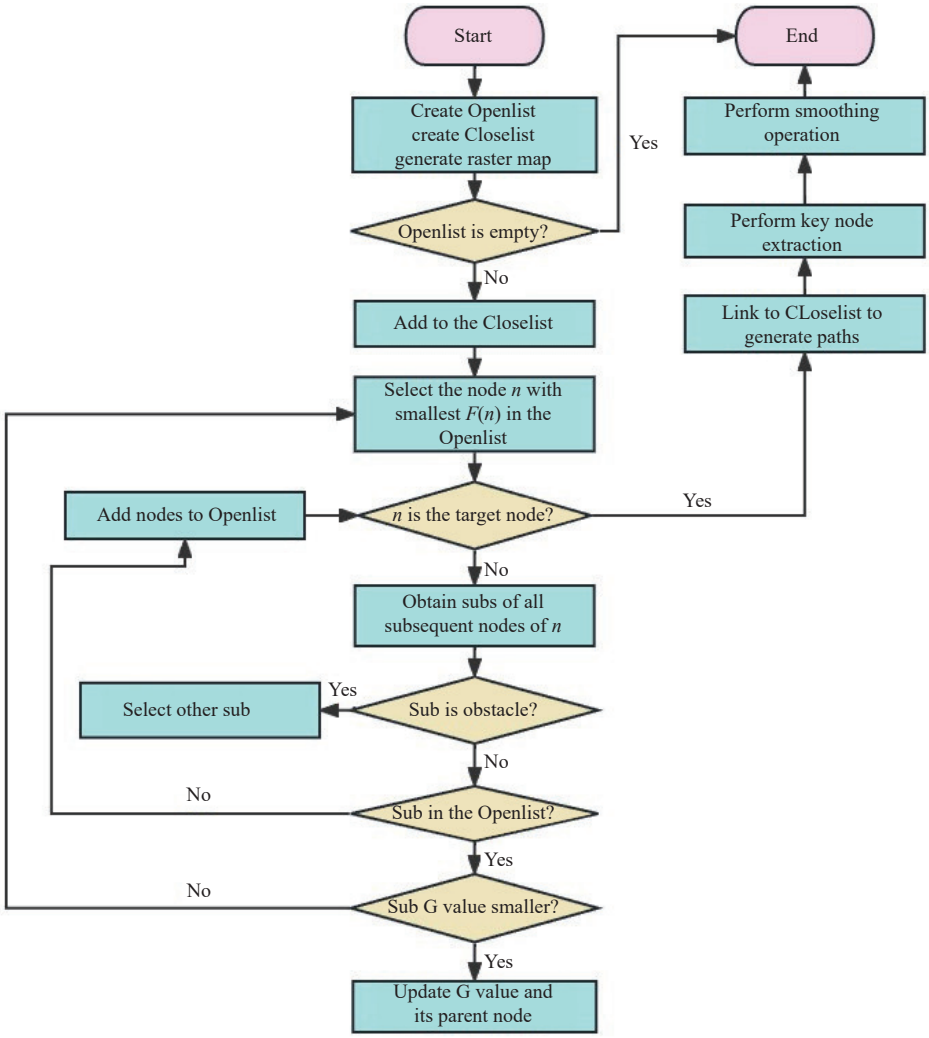

Figure 7 Flowchart of the specific steps in the improved A* algorithm

maximum climbing capability; for this study, the Thunder Mini four-wheel differential drive robot has a maximum climbing capability of 0.013, thus S is set to 0.013. Selecting the appropriate parameter combination is crucial to ensure the algorithm's performance when optimizing complex algorithms. To ensure the validity and reliability of the experimental results, this study references the parameter settings from existing literature. Yan et al.[21] conducted detailed analysis and experimental validation of key parameters for path planning algorithms in their research, demonstrating the superiority of specific parameter combinations in complex environments. Therefore, this study adopts the parameter settings from Yan et al.'s research as an initial reference. The parameters and their ranges were tested on a 100×50 grid map. The experimental results are listed in Table 1, and the optimal parameter combinations are presented in Table 2.

The experiments were performed in different environments to assess the effectiveness of the improved A* algorithm. The simulation experiments used a three-dimensional grid map, where purple grids represent the starting nodes, and green grids represent the target nodes. The experiments were conducted in two different-sized environments: 200×200 and 100×100, both with a maximum vertical height of 15 m in the three-dimensional grid map environment.

The parameters for the improved A* algorithm in the simulation experiments are specified in Table 2, and the results are presented in Figures 8 and 9. Further comparisons of path length, operation time, total number of nodes, paths for poultry observations, and paths for poultry activity points are listed in Table 3.

After 50 simulation runs, it is evident that the improved A* algorithm, when compared to the traditional A* algorithm, is better suited for the wild livestock farm environment. While there are minimal differences in terms of path length and operation time, the improved A* algorithm significantly outperforms the traditional A* algorithm in livestock observation length. It excels in avoiding livestock activity areas and results in smoother path planning.

Table 1 Parameter testing experimental results

Proportionality factor of distance cost	Proportionality factor of potential field	Repulsion coefficient of potential field	Gravitational weight	Repulsive weight	Path length/m	Observation length/m
0.7	0.9	1..0	1.1	2	90.54	0
0.7	1.0	1.1	0.9	3	90.21	0.23
0.7	1.1	0.9	1.0	4	90.55	3.11
0.8	0.9	1.0	1.1	2	93.56	4.96
0.8	1.0	1.0	1.0	3	94.01	6.54
0.8	1.1	0.9	1.0	4	100.23	6.91
0.9	0.9	1.0	1.1	2	98.23	6.21
0.9	1.0	1.1	0.9	3	97.42	6.02
0.9	1.1	0.9	1.0	4	98.62	6.33

Table 2 Parameter of algorithm

Parameters	α	β	η	γ	μ	d_0	S
Values	0.8	1.0	1.0	1.0	3.0	5.0	0.013

To further investigate the advantages of the improved A* algorithm, a second set of experiments was conducted. These experiments started with 40×40 maps and increased in size in steps of 20 in both length and width. They compared the improved A* algorithm to the traditional A* algorithm to confirm the benefits of the improved A* algorithm. The starting and target points were set in corresponding positions on seven maps, as indicated in Table 4.

These findings, based on 50 simulation runs and the additional experiments, demonstrate the advantages of the improved A* algorithm for the wild livestock farm environment.

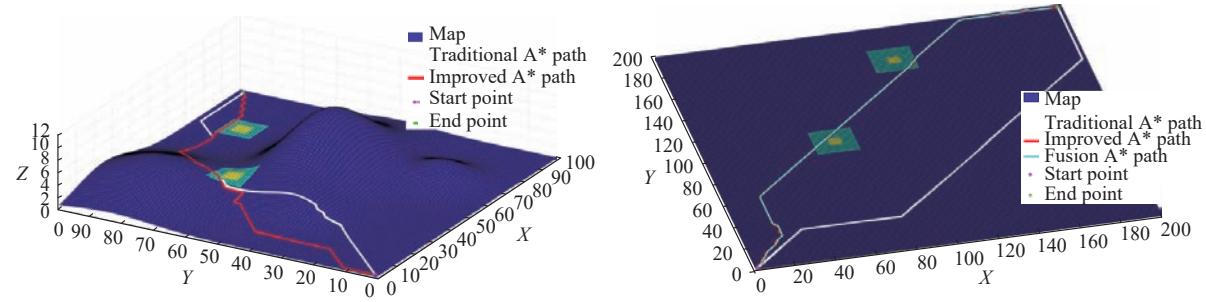

a. Comparison of improved A* (red) and traditional A* (white) and 3D view

b. Comparison of improved A* (cyan) after smoothing and traditional A* (blue) and 2D view

Figure 8 Comparison results of the experiment in 200×200 grid map

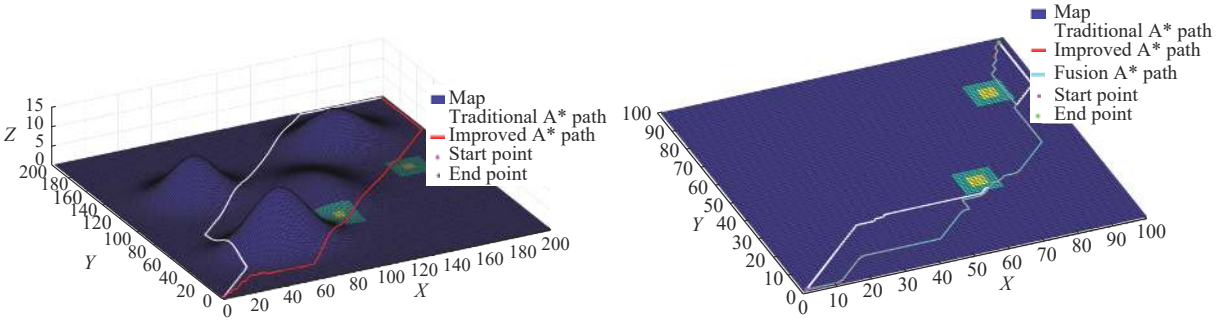

a. Comparison of improved A* (red) and traditional A* (white) and 3D view

b. Comparison of improved A* (cyan) after smoothing and traditional A* (blue) and 2D view

Figure 9 Comparison results of the experiment in 100×100 grid map

Table 3 Performance comparison of the improved A* and traditional A* algorithms

Map size	Algorithm	Path length/m	Operation time/s	Total nodes	Observation length/m	Activity area/m
200×200	Traditional A*	305.8894	1.1304	8855	0	0
	Improved A*	307.7889	0.1384	627	32.1126	0
100×100	Traditional A*	160.3675	0.5124	469	7.6568	0
	Improved A*	163.2965	0.1078	300	17.6568	0

Table 4 Coordinates of start and end points in maps of different sizes

Map size	Start point	End point
40×40	(2, 2)	(38, 38)
60×60	(2, 2)	(58, 58)
80×80	(2, 2)	(78, 78)
100×100	(2, 2)	(98, 98)
120×120	(2, 2)	(118, 118)
140×140	(2, 2)	(138, 138)
160×160	(2, 2)	(158, 158)

The simulation results obtain the A-star algorithm and the improved A-star algorithm in the eight specification graphs corresponding to the path lengths, as shown in Figure 10; explore nodes and their logarithmic scale graphs, as shown in Figure 11; calculate the time of its logarithmic scale graph, as shown in Figure 12.

It is evident that the traditional A* algorithm exhibits exponential growth in computation time and total node count as the map size increases, whereas the improved A* algorithm, with optimized search neighborhoods, significantly reduces the number of explored nodes and computation time. When compared to the traditional A* algorithm, with almost the same total distance, the improved A* algorithm reduces the number of nodes by over 61.0% and decreases the runtime by 69.4%.

As the map size increases, the effectiveness of the improved A* algorithm becomes more pronounced. In summary, the enhanced A* algorithm consistently outperforms the traditional A* algorithm in all scenarios, aligning better with the requirements of the wild animal farming environment while offering superior computation time and exploration node efficiency.

The satellite map experiments were further conducted in a common field-based livestock farming environment. The central coordinates of the experimental scenario were (119°8′40.81″E, 49°24′31.46″N), covering an area of 500×500 m^2 with elevations ranging from 610 to 628 m and significant terrain variations. Matlab was utilized to construct a three-dimensional grid map based on Digital Elevation Model (DEM) data, as shown in Figure 13.

The starting position was set at coordinates (2, 2), and the target position was defined as (498, 498). The parameters for the improved A* algorithm during the experiment remained consistent with those used in the previous simulations, as outlined in Table 2. The results, as illustrated in Figure 14, include a detailed comparison of path length, operational time, total node count, livestock observation paths, and livestock activity point paths, as presented in Table 5.

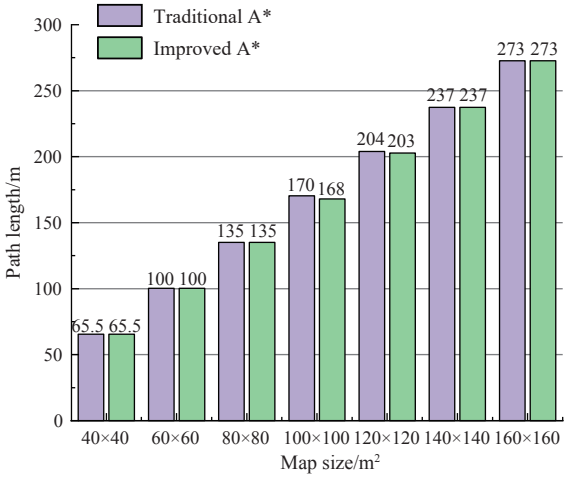

Figure 10 Comparison of path length between traditional A* and improved A*

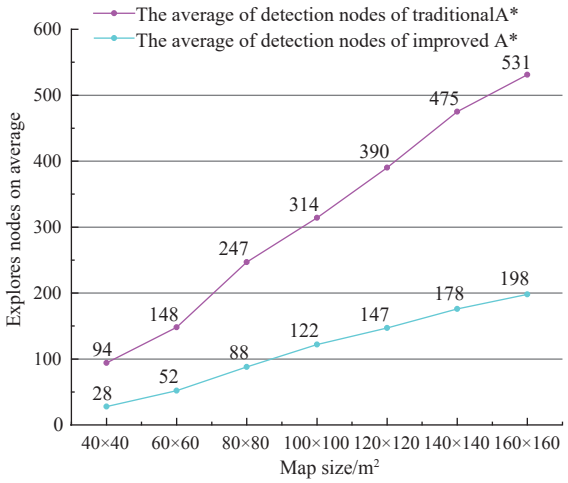

Figure 11 Comparison of explore node between traditional A* and improved A*

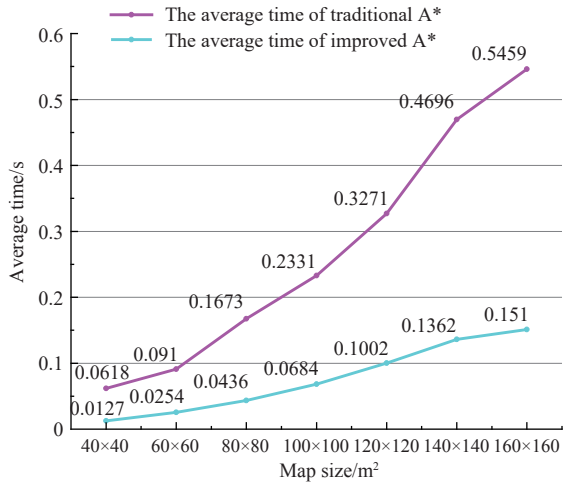

Figure 12 Comparison of operation time between traditional A* and improved A*

After 50 simulations, it becomes evident that, when compared to the traditional A* algorithm, the improved A* algorithm is better suited for field-based livestock farming environments. In scenarios where there is little difference in terms of path length and operational time, the improved A* algorithm significantly outperforms the traditional A* algorithm in terms of livestock observation distance and the avoidance of entering livestock activity areas.

To further validate the performance and practicality of the improved A* algorithm in real-world conditions, tests were conducted in an actual field-based livestock farming environment. The Thunder Mini four-wheel differential drive mobile robot, as shown in Figure 15a, was used in these experiments. The robot measures 0.730 m in length, 0.570 m in width, and 0.606 m in height. It is equipped with a Velodyne Puck 16-line LiDAR for map construction and features an i5-12400F processor with 32 GB of RAM for navigation, localization, and mapping. The Noetic version of ROS and Ubuntu 20.04 operating system were utilized.

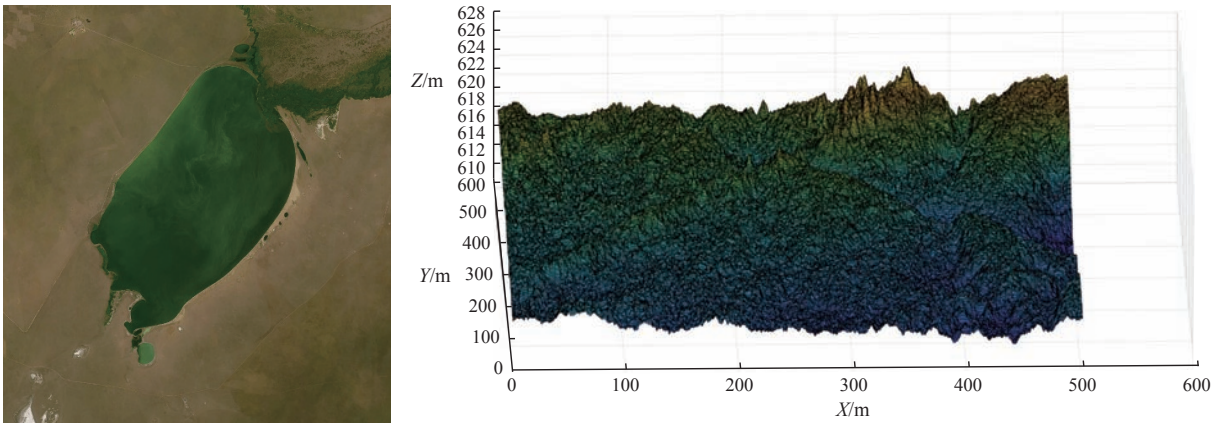

Figure 13 Three-dimensional elevation model of experimental map

As illustrated in Figure 16a, the experiment parameters were set with a starting position of (91.31 m, 80.03 m, 0.02 m) and a goal position of (20.27 m, 69.56 m, 0.50 m). The map resolution was 0.05 m, the maximum linear velocity was 0.50 m/s, the maximum angular velocity was 2.75 rad/s, the maximum linear acceleration was 1.0 m/s^2, and the maximum angular acceleration was 3.2 rad/s^2. The parameters of the improved A* algorithm were consistent with those used in the simulation experiments, as detailed in Table 2.

Figure 15a provides a detailed view of the key electronic components integrated within the robot. A 3D environmental model of the field-based livestock farm was constructed using a 3D LiDAR, as shown in Figure 15b. The initial and target positions are shown in Figures 15c and 15d. Figure 15e depicts the livestock activity area. Figure 15f shows the environment encountered by the mobile robot during operation. The path planning results of the traditional A* and improved A* algorithms are illustrated in Figures 16a-16c.

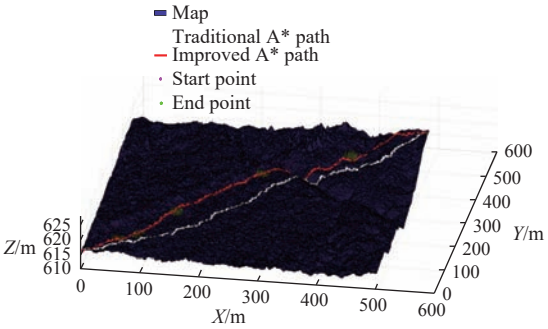

Figure 14 Comparison results of the experiment in 500×500 grid map

Table 6 lists the averages from 20 tests conducted using the Thunder Mini four-wheel differential mobile robot in a field-based livestock farm. From the data in Table 6, it can be deduced that the improved A* algorithm reduces computation time by 48.70% compared to the traditional A* algorithm, while maintaining a comparable path length. Additionally, the improved A* algorithm reduces the total number of search nodes by 37.90%. Moreover, the improved A* algorithm significantly increases the length of livestock observation without entering designated livestock activity areas, surpassing the traditional A* algorithm.

Table 5 Performance comparison of the improved A* and traditional A* algorithms in 500×500 grid map

Map size	Algorithm	Path length/m	Operation time/s	Total nodes	Observation length/m	Activity area/m
500×500	Traditional A*	832.55	330.98	11 220	0	0
	Improved A*	840.05	23.19	906	104.78	0

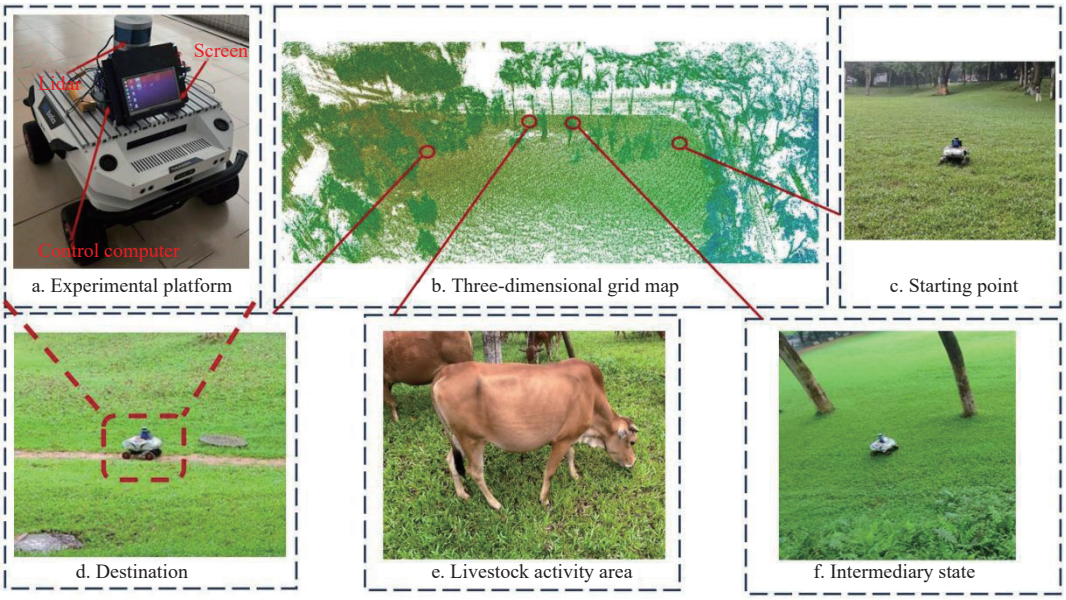

Figure 15 Experimental equipment and environment

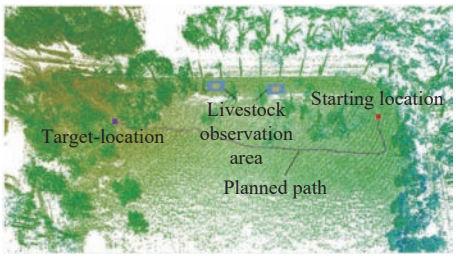

a. Traditional A* algorithm planning path

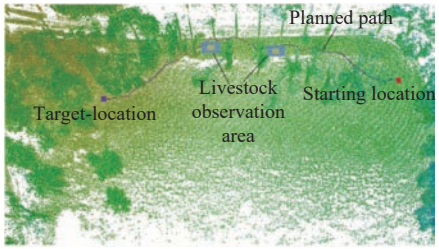

b. Improved A* algorithm planning path

c. Improved A* algorithm planning path of the side view

Figure 16 Planned trajectories of different algorithms

Table 6 Performance comparison of the improved A* and traditional A* algorithms in wild livestock farm

Map size	Algorithm	Path length/m	Operation time/s	Total nodes	Observation length/m	Activity area/m
50×100	Traditional A*	93.56	1.811	153	0	0
	Improved A*	95.06	0.929	95	7.93	0

4 Conclusions

The proposed method is designed to enhance the widely used A-sta (A*) algorithm by introducing a novel heuristic function. It takes into account the impact of terrain slopes in the outdoor environment on vehicle navigation. Based on the distribution of target nodes and obstacles, the search neighborhood in the traditional A* algorithm is adjusted from 8 nodes to 3 nodes, effectively eliminating redundant expansion nodes. Furthermore, this method introduces weighted factors and an artificial potential field into the evaluation function of the traditional A* algorithm. This enhances the algorithm's search direction information, allowing it to efficiently observe livestock without disturbing them. Consequently, it reduces the number of expansion nodes and search time, thereby improving the A* algorithm's performance.

In comparison to traditional heuristic functions that only consider distance, this approach considers livestock information specific to the outdoor farming environment, making it more

suitable for livestock farming scenarios. The improved algorithm provides shorter path calculation times, reduces unnecessary nodes, and enhances the algorithm's operational efficiency.

The algorithm's limitations are important to consider for further research and improvement. Here's a summary of the limitations and potential future work:

Limitations:

1) The algorithm is not suitable for complex dynamic scenarios, as it may not handle rapidly changing conditions.

2) The algorithm may occasionally get trapped in corner cases during neighborhood search, leading to redundant nodes. However, simulation results show that the probability of getting stuck in random environments is low.

Future Work:

1) Investigate the algorithm's performance in complex dynamic scenarios common in outdoor livestock environments to ensure its robustness.

2) Explore the integration of techniques like key point extraction to prevent getting stuck in corner locations and to reduce redundant nodes, ultimately improving algorithm efficiency.

3) Conduct comparative studies between the improved algorithm and other recent algorithms for mobile robot path planning. This will help further validate the algorithm's effectiveness and identify areas for further improvement.

Acknowledgements

This study was supported by the Subject construction projects in specific universities (Grant No. 2023B10564003) and the Science and Technology Rural Commissioner Project of Guangzhou (Grant No. 20212100026).

[References]

[1] Uehleke R, Seifert S, Hüttel S. Do animal welfare schemes promote better animal health? An empirical investigation of german pork production. Livestock Science, 2021; 247: 104481.

[2] Zhou J B. Animal welfare farming and the development of modern animal husbandry in Jinzhong City. The Chinese Livestock and Poultry Breeding, 2021; 17(5): 6–7. (in Chinese)

[3] Temple D, Manteca X, Velarde A, Dalmau A. Assessment of animal welfare through behavioural parameters in Iberian pigs in intensive and extensive conditions. Applied Animal Behaviour Science, 2011; 131(1-2): 29–39.

[4] Wang T, Xu X B, Wang C, Li Z, Li D L. From smart farming towards unmanned farms: A new mode of agricultural production. Agriculture, 2021; 11(2): 145.

[5] Li D L, Yang H. State-of-the-art review for internet of thingsin agriculture. Transactions of the CSAM, 2018; 49(1): 1–20. (in Chinese)

[6] Nie P C, Zhang H, Geng H L, Wang Z, He Y. Current situation and development trend of agricultural internet of things technology. Journal of Zhejiang University (Agriculture & Life Sciences), 2021; 47(2): 135–146. (in Chinese)

[7] Sun J L, Li D H, Xu S W, Wu W B, Yang Y P. Development strategy of agricultural big data and information infrastructure. Strategic Study of CAE, 2021; 23(4): 10–18. (in Chinese)

[8] Lan Y B, Wang T W, Chen S D, Deng X L. Agricultural artificial intelligence technology: Wings of modern agricultural science and technology. Journal of South China Agricultural University, 2020; 41(6): 1–13. (in Chinese)

[9] Tian N, Yang X W, Shan D L, Wu J C. Status and prospect of digital agriculture in China. Journal of Chinese Agricultural Mechanization, 2019; 40(4): 210–213. (in Chinese)

[10] Zheng D R. Smart agriculture development in China: Present situation, problems and countermeasures. Agricultural Economy, 2020; 1: 12–14.

[11] Poultry Patrol, 2019. Available: https://poultrypatrol.com/?page_id=472. Accessed on [2021-08-06].

[12] ChickenBoy, 2021. Available: https://faromatics.com/. Accessed on [2021-08-06].

[13] Feng Q C, Wang X. Design of disinfection robot for livestock breeding. Procedia Computer Science, 2020; 166: 310–314.

[14] Wu T Y, Xu J H, Liu J Y. Cross-country path planning based on improved ant colony algorithm. Journal of Computer Applications, 2013; 33(4): 1157–1160. (in Chinese)

[15] Ji Y, Tanaka Y, Tamura Y, Kimura M, Umemura A, Kaneshima Y, et al. Adaptive motion planning based on vehicle characteristics and regulations for off-road UGVs. IEEE Transactions on Industrial Informatics, 2018; 15(1): 599–611.

[16] Tian H Q, Wang J Q, Huang H Y, Ding F. Probabilistic road-map method for path planning of intelligent vehicle based on artificial potential field model in China off-road environment. Acta Armamentarii, 2021; 42(7): 1496–1505. (in Chinese)

[17] Zhao M T. Path planning method for ground unmanned plat-form in cross-country environment. Master dissertation. Beijing: North China University of Technology, 2021; 59p. (in Chinese)

[18] Wang K, Wang H, Wu B. Optimal off-road path planning based on tabu table. In: Proceedings of the 8th China Command and Control Conference, Beijing, 2020; pp.380–385. (in Chinese)

[19] Hart P E, Nilsson N J, Raphael B. A formal basis for the heuristic determination of minimum cost paths. IEEE Transactions on Systems Science and Cybernetics, 1968; 4(2): 100–107.

[20] Li D F, Liu M, Zhang J P, Cheng E L. An improved A* algorithm applicable for campus navigation system. In: 2015 International Conference on Network and Information Systems for Computers, Wuhan: IEEE, pp.588–591. doi: 10.1109/ICNISC.2015.72.

[21] Yan X D, Chang T Q. Guo L B. Research on path planning of unmanned vehicle in off-road battlefield environment. Journal of Ordnance Equipment Engineering, 2022; 43(10): 288–293. (in Chinese)